Available online at www.sciencedirect.com
ScienceDirect
European Journal of Mechanics B/Fluids 26 (2007) 236–257

Manipulation of the reverse-flow region downstream of a fence by spanwise vortices

H.A. Siller [a,*], H.-H. Fernholz [b]

[a] *DLR, Institute of Propulsion Technology, Engine Acoustics, Berlin, Germany*
[b] *Hermann-Föttinger-Institut für Strömungsmechanik, TU Berlin, Germany*

Received 25 August 2005; received in revised form 20 December 2005; accepted 9 May 2006

Available online 14 July 2006

Abstract

The experimental investigation of a turbulent separated flow over a fence is presented. By introducing a periodic disturbance upstream of the separation region in front of the fence, the time averaged length of the separation region downstream of the fence was reduced by as much as 40%. Two types of flow manipulation were applied: an oscillating cross-flow with zero net mass-flux through a spanwise slot in the floor of the test section and a spanwise oriented, oscillating spoiler. The cross-flow was generated by a loudspeaker system connected to a chamber underneath the spanwise slot. Both types of flow manipulation generate spanwise vortices at the fence that convect into the region downstream of the fence where they enhance the mixing in the shear layer and reduce the time mean length of the reverse-flow region downstream of the fence. Velocity profiles phase averaged with respect to the forcing frequency and phase triggered flow visualisations show that the spanwise vortices cause the long reverse-flow region of the unmanipulated flow to break up into separate smaller regions. While the time mean length of the reverse-flow region is reduced in the manipulated case, the length of the region where instantaneous reverse-flow occurs is not changed. The data presented include wall pulsed-wire measurements of the wall shear-stress and its turbulent fluctuations, and LDA measurements of the streamwise and the wall-normal velocity components and turbulent stresses.

Keywords: Turbulent flow; Separated flow; Flow manipulation; Jet actuator; Flow control

1. Introduction

The generic case of a turbulent flow over a two-dimensional sharp edged fence was investigated for Reynolds numbers Re_h of 10 500 based on obstacle height and mean flow velocity. First, the flow upstream of the fence [1] and the natural turbulent flow over and downstream of the fence were investigated [2]. Spectra of velocity fluctuations in the shear layer over the separation region downstream of the fence showed that a preferred vortex-shedding frequency exists.

Different methods of reducing the reverse-flow region downstream of the fence by active manipulation were tested. Two different actuators were used upstream of the fence: an oscillating spoiler [3], and a two-dimensional oscillating

* Corresponding author. DLR, Müller-Breslau-Str. 8, D-10623 Berlin, Germany. Tel.: +4930 310 006 57; fax: +4930 310 006 39.
E-mail addresses: henri.siller@dlr.de (H.A. Siller), fernholz@pi.tu-berlin.de (H.-H. Fernholz).

0997-7546/$ – see front matter
doi:10.1016/j.euromechflu.2006.05.005

jet generated in a spanwise oriented slot by a loudspeaker. Both devices introduce a strong perturbation into the flow and generate spanwise vortices similar to starting vortices. The disturbances have the greatest effect on the length of the reverse-flow region when the frequency is close to the natural vortex-shedding frequency. Also, the position where the disturbance should be introduced was optimised and the largest reductions of the downstream recirculation region were achieved with the actuators positioned slightly upstream of the separation region in front of the fence.

Huppertz and Fernholz [4] investigated the flow over a swept fence. They used both the upstream slot actuator and a low-amplitude forcing at the fence tip that affected the vortex roll up of the shear layer by excitation of the Kelvin–Helmholtz instability.

1.1. Separated two-dimensional turbulent flow

The flow over a two-dimensional fence falls into the category of separated, two-dimensional turbulent flows. A review of experimental work in this field is given by Sympson [5]. Turbulent flow is by its nature always three-dimensional. However, it can be described as being *spanwise invariant*, if the gradients of the mean velocity components in the spanwise direction can be neglected [6]. An experiment that fulfils this condition needs uniform upstream conditions and a sufficiently large aspect ratio of the model.

Fernholz [7] discussed pressure and shear driven flow separation. In the case of pressure driven separation, the separation line is not fixed in space and can oscillate freely. Examples for this behaviour are the trailing-edge stall on aerofoils and the separation region upstream of surface-mounted obstacles. In the case of shear-driven separation, the separation line is fixed and such flows are therefore more easily accessible to an experimental or numerical study.

The flow over prismatic obstacles mounted on a flat plate features in addition to the separation at a sharp edge a pressure driven separation region upstream of the obstacle. The boundary layer along the plate and the upstream separation region will interact with the separation region downstream. Depending on the ratio of the object height to its length in the streamwise direction, a secondary separation region may form on top of the obstacle itself. A fence with a sharp edge is the lower limiting case for this class of flows.

Experiments with a fence flow were described by Good and Joubert [8]. They showed measurements of the mean flow-field upstream and downstream of a two-dimensional fence using static pressure probes. The emphasis was on the determination of the form drag of the fence. Later studies targeted the correct prediction of the fence drag, Ranga Raju et al. (e.g. [9]) and Castro and Fackrell [10]. Durst and Rastogi [11] made an experimental investigation of the separation lengths downstream of two-dimensional fences in order to test their numerical codes. The re-attachment length and the heat transfer downstream of a fence under the influence of different levels of free-stream turbulence were investigated by Žukauskas and Pedišius [12]. Wagner [13] studied coherent structures in the near-wall region of the turbulent separated flow downstream of a fence with the experimental set-up used in the present study. Schmidt [14], and Ullum et al. [15] performed detailed measurements of the turbulent flow over a fence at moderate Reynolds numbers and successfully manipulated the length of the downstream separation region by periodic forcing. Preliminary results of the present study have been published in Siller and Fernholz [16] and Siller and Fernholz [3], a large-eddy-simulation of the natural, unperturbed flow was given by Orellano [17].

1.2. Active manipulation of turbulent separated flows

Experimental investigations of flow control applications on separated flows have been made in a number of different flow configurations with different levels of complexity. Frequently, flow control methods are employed to induce early re-attachment of the separated flow (i.e. to shorten the separation region). A review of applications of separation control is given by Gad-el Hak and Bushnell [18], however with the emphasis on pressure driven separation. In the past, the high Reynolds numbers of such cases prohibited numerical investigations. However, this situation has improved in recent years. Orellano and Wengle [19], for example, calculated a large-eddy simulation of the experiment by Schmidt [14] with a Reynolds number of 3000 based on the free-stream velocity and the obstacle height.

Active methods of flow control, like oscillating mechanical devices, oscillatory blowing, or zero net mass-flux actuators use instabilities inherent of the flow. They introduce disturbances with a specific frequency or Strouhal number into the flow that is tuned to the most receptive frequency of the flow field. There exist at least two different instability mechanisms, the Kelvin–Helmholtz instability, and the shedding-type instability described by Sigurdson [20]. Even when both mechanisms occur together, the respective Strouhal numbers are usually well separated and, depending

on the state of the flow, one mechanism will precede over the other. The question remains, however, which Strouhal number will lead to the greatest reduction of the separation length.

1.2.1. Oscillatory manipulation of a boundary layer flow

Miau and Chou [21] and Miau et al. [22] investigated the effect of an oscillating, vertical plate in a turbulent boundary layer. During one oscillation cycle, the plate moves from the fully retracted position to its maximum height and back. They found two states of the flow, depending on the oscillation frequency. Below a critical frequency, the separation bubble behind the fence has enough time to build up to a size that it would have in a stationary situation. The boundary layer thickness measured at a station downstream of the wake of the fence oscillates sinusoidally. Above the critical frequency, the vorticity generated at the fence tip is caught in the wake of the plate and a vortex is shed when the plate retracts. The boundary layer downstream remains relatively thin over most of the oscillation cycle, apart from a peak caused by the passing of the vortex. Also, the minimum of the wall pressure measured behind the oscillating fence is lower than in the stationary case for supercritical frequencies. With increasing frequency, it is further reduced and moves upstream towards the fence, indicating that the fence tip vortex reduces its size.

The oscillating spoiler used in the present work with its sharp tip presents a similar situation as the oscillating vertical plate. The reduced frequency of the oscillating spoiler calculated with the spoiler amplitude corresponds to a value of $St_H = 0.01$ and is just above the critical frequency of 0.009 found by Miau and Chou [21].

1.2.2. The shedding type instability of a separation region

Sigurdson [20] describes the *shedding type instability*, that occurs in fully turbulent separated flows. Comparing experimental results, he concludes that the optimal forcing frequency that leads to the greatest reduction of the re-attachment length scales with the maximum height of the separation bubble $h_{\max}$ and the free-stream velocity at separation $\overline{u_s}$:

$$St_s = \frac{f_s h_{\max}}{\overline{u_s}} = 0.08 \pm 0.01. \tag{1}$$

This value is close to the Strouhal number of natural vortex shedding from the separation bubble in a wide range of different experiments [20]. The connection between the natural shedding frequency and the optimal forcing frequency has been confirmed by Chun and Sung [23] for a fully turbulent backward-facing step flow and by the present study.

In a laminar or transitional flow, the optimal reduction of the separation region is achieved when the flow is forced with the most unstable frequency of the Kelvin–Helmholtz instability. Even for very low amplitude forcing, the roll-up of the shear layer is amplified. Transition to turbulence is induced and the rate of entrainment increases, leading to a reduced length of the separation region.

In a turbulent separation bubble, the structures that contain most of the energy are the large vortices which are being shed from the separation bubble. By forcing with amplitudes in the order of the free-stream flow velocity, spanwise vortices with a diameter in the order of the height of the separation region are generated that efficiently mix the flow and reduce the mean separation length. In the experiments described here, the reverse-flow region downstream of the fence was reduced by 40%.

The aim of this investigation was to reduce the re-attachment length downstream of the fence l_r as much as possible for the given geometry at a Reynolds number $Re_h = 10\,500$. A parameter study was performed in order to find the optimum distance between the actuator position and the fence l_{sf}, the Strouhal number St_h, and the non-dimensional amplitude, the Euler number Eu, which gives the greatest reduction of the re-attachment length. The length of the reverse-flow region downstream of the fence l_r (i.e. the distance along the centre line of the test section between the fence and re-attachment) was determined by surface flow-visualisations.

Once optimal values for l_{sf}, St_h, and Eu had been established, the optimised flow was investigated further: The properties of the oscillating jet itself were investigated using flow visualisations as well as laser-Doppler measurements. In the flow field up- and downstream of the fence, the flow was visualised using the smoke-wire technique. Wall shear-stress measurements downstream of the fence were performed using wall pulsed-wire probes and a surface fence for streamwise and spanwise surveys, respectively. Boundary-layer profiles were measured at identical positions for the natural and the manipulated flow. Phase averaged velocity and vorticity fields and frequency spectra were calculated from the LDA data of the forced flow.

Because of the unsteady nature of the two flows, the dynamic behaviour is illustrated using flow visualisation techniques. Quantitative data of the wall pressure, the wall shear-stress and the flow velocity, the time averaged

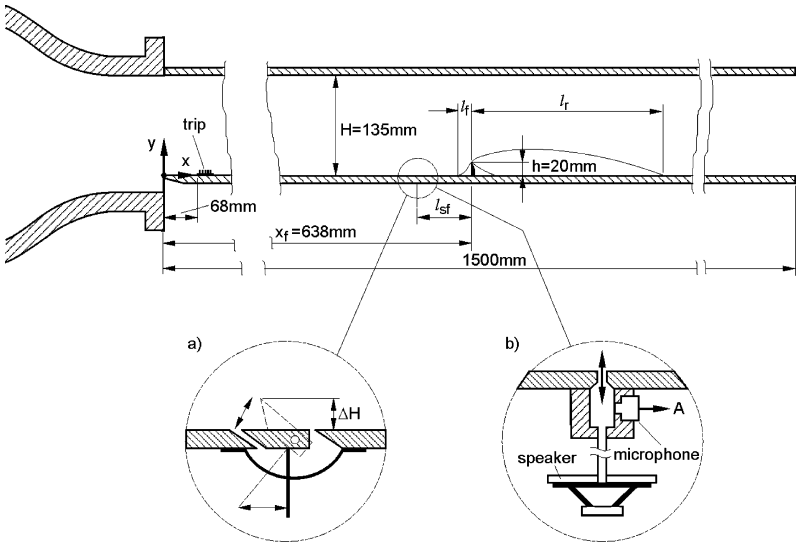

Fig. 1. Experimental set-up: fence flow with upstream manipulation by either an oscillating spoiler or a zero net mass-flux actuator.

velocity components $\bar{u}$ and $\bar{v}$ and the turbulent quantities $\overline{u'^2}$, $\overline{v'^2}$ and $\overline{u'v'}$ are shown together with frequency spectra in the shear layers and quantities calculated from the velocity profiles, such as boundary layer and shear layer thicknesses.

2. Experimental set-up and methods

2.1. Wind tunnel and test section

The measurements were performed in the test section of a blower-type wind tunnel shown in Fig. 1. The test section had a rectangular cross-section of 440 × 135 mm and a length of 1500 mm. One side wall and the roof of the test section were made of glass to allow optical access. The floor plate, where the fence was mounted, was raised by 17 mm above the downstream edge of the wind-tunnel nozzle in order to remove the nozzle boundary layer.

In order to generate a uniform flow at the entrance of the test section, the settling chamber was equipped with a non-woven filter mat and a single, precisely manufactured perforated metal plate (64% openness). The nozzle had a contraction ratio of 5.3.

The fence had a height of $h = 20$ mm and a sharp upper edge with a backward chamfer. It was mounted at $x_f = 638.0$ mm downstream of the leading edge and the ratio of wind tunnel width to fence height was 22. The upstream laminar boundary layer was tripped by a Velcro tape of 2.6 mm height located 67 mm downstream of the elliptical nose of the floor plate. The distance from the origin of the turbulent boundary layer to the position of the fence was $\Delta x_f/h = 28.5$ and may be considered large compared with $l_f/h = 0.65$, the ratio between the distance from the mean separation line upstream of the fence to the fence l_f and the fence height h. The ratio of boundary layer thickness and fence height measured at the fence position in its absence was $\delta_{99\%}/h = 0.8$.

The actuator was positioned upstream of the fence. Either a mechanically oscillating spoiler or an oscillating cross-flow through a spanwise slot could be inserted. The optimal position of the actuator for a maximum reduction of the recirculation length downstream of the fence l_{sf} was determined by flow-visualisation experiments. It was the same distance for both devices, approximately 1.75 fence heights h upstream of the fence.

2.2. Measurement techniques

Only flow visualisation was used to investigate the flow manipulated by the oscillating spoiler. For the case with the oscillating zero net mass-flux jet, detailed quantitative flow measurements were made. For both cases, the flow was visualised by means of the smoke-wire technique, using a flash light synchronised with the phase of the actuator motion. The length of the recirculation region was determined by surface flow visualisation with pigmented oil. The free-stream velocity was monitored by a Pitot-static tube mounted near the entrance of the test section.

The u and v components of the mean and fluctuating velocity were measured using a Dantec two-component fibre-optic LDA system. It was powered by a 300 mW argon-ion laser and operated in backscatter mode. Two Dantec burst-spectrum analyser (BSA) modules performed the data conversion in continuous mode. Coincidence checking was performed in private/private mode. A frequency shift was applied in order to discriminate between forward and backward flow. The focal length of the probe was 600 mm and the measuring volume was an ellipsoid of revolution with a length of 1.4 mm and a diameter of 88 μm.

Measurement errors were checked by measuring a velocity profile under identical conditions with the LDA system and a hot-wire anemometer in a flow region without reverse flow. The differences between the two measurements were below +2.5%–3.5% for the mean value and below 5.0% for the fluctuating component of the velocity except for the region very close to the wall, where the hot-wire is known to give erroneous results.

The wall shear-stress τ_w and the reverse-flow factor at the wall χ_w were measured using a wall pulsed-wire (Bradbury and Castro [24] and Castro [25]). χ_w is the ratio of heat pulses detected at the upstream wire, which indicate reverse-flow, to the total number of heat pulses at both sensor wires. The wall pulsed-wire probe was set up for high sensitivity, using sensor wires with a diameter of 2.5 μm and an active length of 2.5 mm positioned 0.1 mm above the wall. The sensor wires were 1.4 mm apart in the streamwise direction with the pulser wire in the middle. The pulser wire had a diameter of 5 μm and was 5.0 mm long. The wall pulsed-wire probe was calibrated against a Preston tube [26] in the turbulent boundary layer of the test section with the fence removed.

As an indirect measure of the jet velocity in the slot, the sound-pressure level inside the chamber was permanently monitored using a calibrated electret microphone-capsule. For the experiments with the optimised forcing that led to the greatest reduction of the downstream reverse-flow region, the sound pressure level inside the pressure chamber was constant at $A = 136$ dB.

2.3. The oscillating spoiler

The oscillating spoiler consisted of a narrow spanwise strip of aluminium that could be tilted around an axis (see Fig. 2). Its periodic up- and downward motion was driven by an electric motor, and it was equipped with an opto-electronic device that generated trigger impulses in intervals of 60°over the whole oscillation cycle of the spoiler. These impulses were used to trigger the flash light used for the flow-visualisation. The mechanical spoiler tended to become unstable for higher oscillation frequencies. Its upper frequency limit was at about 25 Hz. This corresponds to a Strouhal number $St_h = 0.06$, which turned out to be close to the optimal forcing frequency of 0.05.

2.4. The oscillating cross-flow with zero net mass-flux

The oscillating cross-flow was generated in a spanwise slot in the floor plate upstream of the fence by a loudspeaker driven with a sinusoidal signal. Fig. 3 shows LDA measurements of the u and v velocity components near the slot exit plotted against the phase angle.

The slot is situated at $l_{sf} = 35$ mm upstream of the fence. It is $s = 1$ mm wide and 392 mm long, spanning 89% of the width $B = 440$ mm of the test section.

Fig. 4 shows the flow with zero net mass-flux through the slot: during its downstroke, the slot acts as a sink and air is drawn into the pressure chamber. During its upward motion, the loudspeaker pushes the air out again generating a two-dimensional jet at the slot exit. Fig. 4 was compiled from phase-averaged LDA measurements. The measurements were triggered by the loud-speaker signal and all data from an interval of $\Delta\varphi = 15°$ was used to form phase averages.

The oscillating cross-flow at the slot exit is nearly homogeneous in spanwise direction: The spanwise distribution of the sound pressure level above the slot was measured with a microphone that could be traversed along the slot. It is uniform to a first approximation with a mean value of $\bar{A} = 131.2$ dB, with fluctuations between +0.3 and −1.0 dB.

3. Reduction of the downstream reverse-flow region

In a fence flow, manipulated by an actuator upstream of the fence, several parameters affect the maximum of the reduction of the time mean recirculation length downstream of the fence. These are (i) amplitude, (ii) frequency, and (iii) the distance of the actuator to the upstream face of the fence. This latter distance will depend on the position of the separation line of the upstream boundary layer. In order to find the optimum set of parameters for the reduction of the

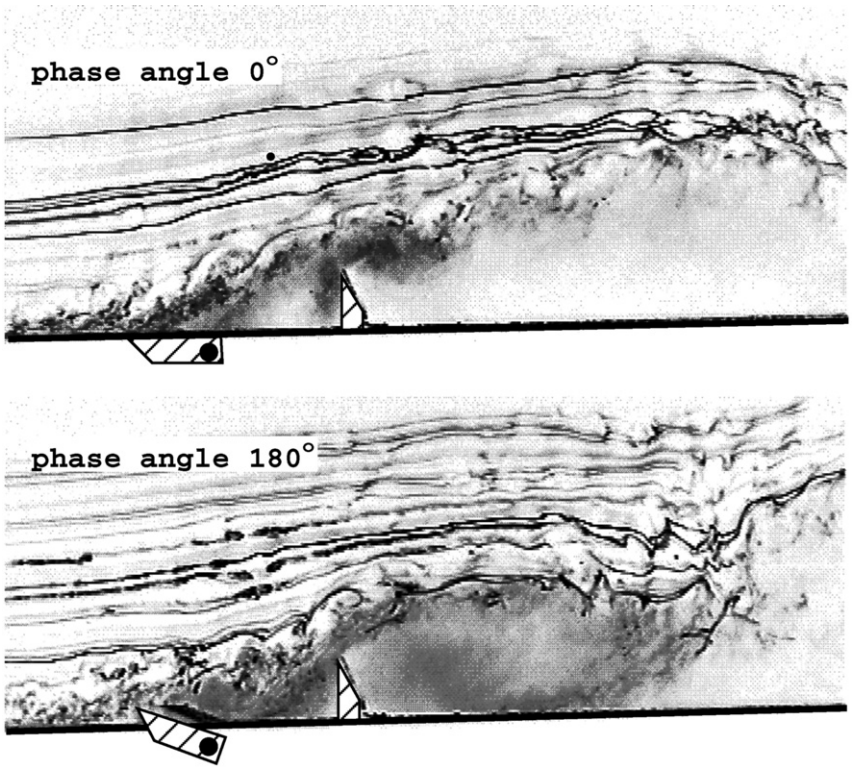

Fig. 2. Smoke-wire flow visualisations of the fence flow with the oscillating spoiler.

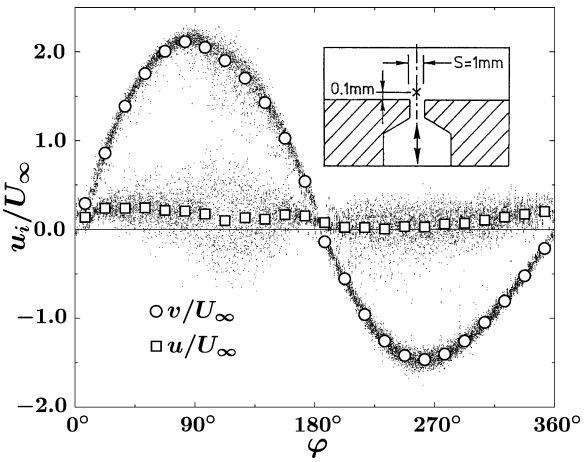

Fig. 3. Phase averaged velocity above the slot. Scattered points: phase averaged within intervals of $\Delta\varphi = 1°$, open symbols: phase averaged within intervals of $\Delta\varphi = 15°$.

downstream separation bubble, optimal values of the Euler number, the Strouhal number, and the actuator location l_{sf} must be determined. This is apparently an iterative procedure. Since the actuator had to be situated upstream of the upstream separation line, a good estimate for the value of l_{sf} between 1.5 and 2.0 could be taken from surface-flow visualisations and later be confirmed for the optimal Euler and Strouhal numbers (see Fig. 5).

The Euler number $Eu = p_a/\rho U_\infty^2$, calculated from the sound pressure level p_a in the actuator slot, is a measure of the amplitude of the forcing. With $l_{sf}/h = 1.75$ and an optimal value of the Strouhal number $St_h = 0.05$ (to be determined below), the length of the time mean recirculation region l_r downstream of the fence can be found

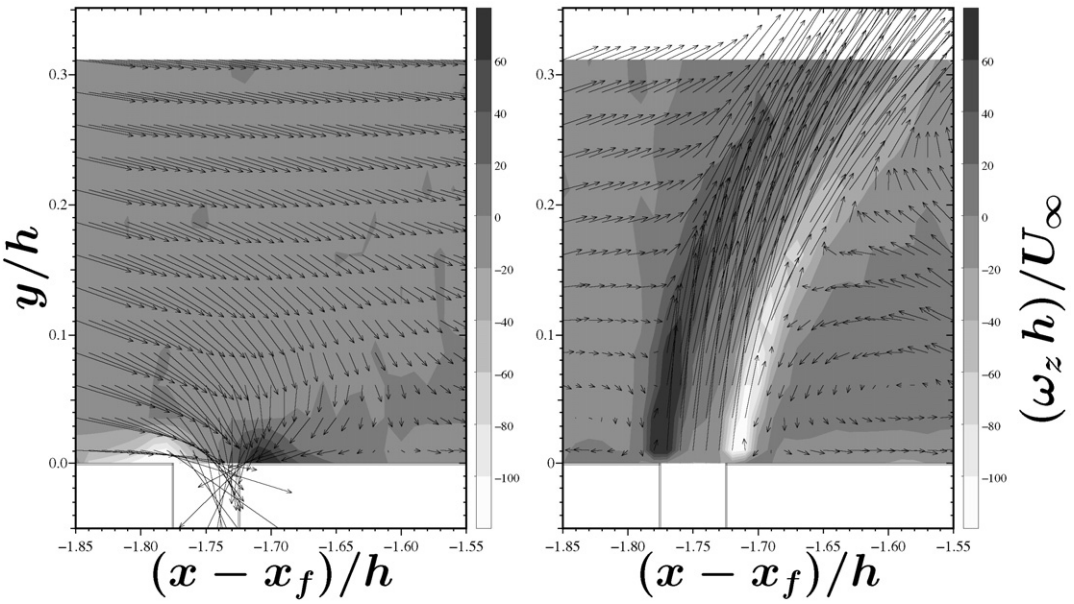

Fig. 4. Velocity and vorticity fields over the slot at $\varphi = 112° \pm 7.5°$ and at $\varphi = 292° \pm 7.5°$.

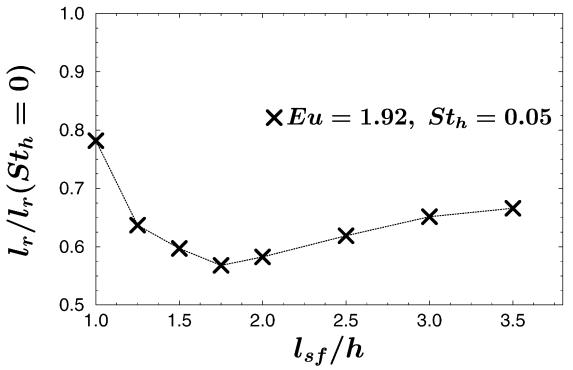

Fig. 5. The length of the separation region l_r scaled with the length l_r $(St_h = 0)$ measured without manipulation as a function of the distance from the slot to the fence l_{sf} for the optimal amplitude and frequency.

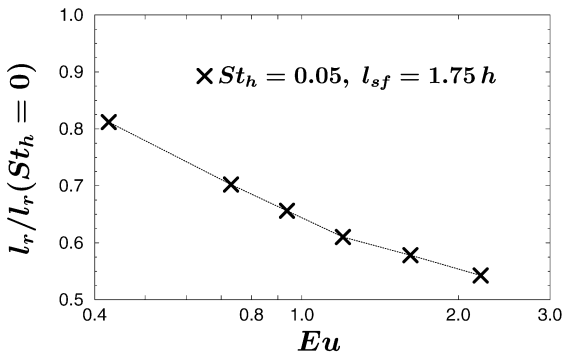

Fig. 6. The ratio l_r / l_r $(St_h = 0)$ as a function of the Euler number for the optimal Strouhal number and distance between the slot and the fence l_{sf}.

experimentally as a function of the Euler number (see Fig. 6). l_r decreases monotonically with increasing Eu. A point, where a further increase of Eu would not reduce l_r further, could not be reached with the present set-up. However, for increasing amplitudes, the oscillating jet will eventually become so strong that its influence on the flow will dominate over that of the fence.

The variation of the actuator frequency, non-dimensionalised as the Strouhal number $St_h = (f\,h)/U_\infty$ shows that there exists an optimal Strouhal number of $St_h \approx 0.05$, where the downstream recirculation region becomes shortest (see Fig. 7). Near $St_h \approx 0.14$, the effect of the flow manipulation almost vanishes and for higher Strouhal numbers, there is another but less pronounced local minimum of the length of the separation region. Also, there is a small influence of the Reynolds number on the length of the reverse flow region, but not on the optimal Strouhal number.

3.1. Flow visualisations

Fig. 8 shows visualisations of the flow over the fence manipulated by the spoiler. The video pictures (taken in increments of 60°) were taken with a stroboscopic lamp that was synchronised with the spoiler actuation mechanism.

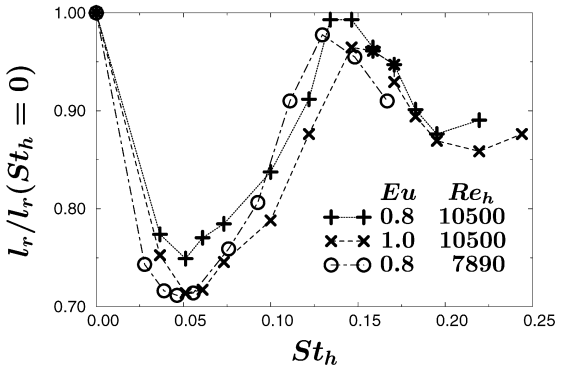

Fig. 7. The length of the separation region l_r scaled with the length l_r $(St_h = 0)$ measured without manipulation as a function of St_h for two different amplitudes and a constant distance of the slot to the fence $l_{sf} = 1.75h$ ($l_{sf} = 2.0h$ for $Re_h = 7890$).

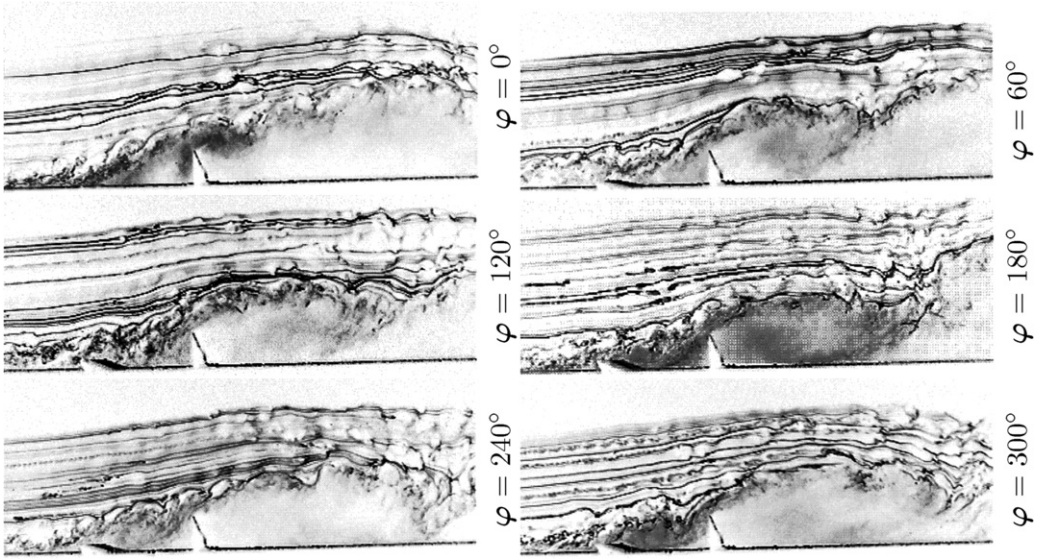

Fig. 8. Phase triggered flow-visualisation of the fence flow with the oscillating spoiler for phase angles 0° to 270° in increments of 60°. The right edges of the images are $8h$ downstream of the fence, the time averaged reattachment position is situated shortly downstream.

The sequence of images shows how a vortex builds up and recedes dynamically downstream of the spoiler. Another large vortex forms at the fence tip and convects through the recirculation region downstream of the fence.

If the oscillating jet is used as the actuator, the flow visualisations show a similar behaviour of the flow. Fig. 9 presents the phase triggered images in increments of 15° of the phase angle. From a large number of images, and also from the velocity measurements in the shear layer, it became apparent, however, that another effect, associated with the sub-harmonic frequency, is present. At each phase angle, two alternative situations may occur, because at almost every second cycle, a very large structure is shed from the downstream recirculation region. Fig. 9 shows the two situations side by side, with the large-structures example shown on the left. The images were chosen as typical of their respective phase angle from a larger number of images. The selection must be considered subjective, however, because the number of samples is too limited for a statistical analysis.

4. Flow structure and frequency spectra

4.1. The natural vortex shedding Strouhal number

The reverse-flow region downstream of the fence is characterised by intense turbulent fluctuations and large vortical structures in the shear layer (see Fig. 10(a)). The largest of these structures impose strong local perturbations on the

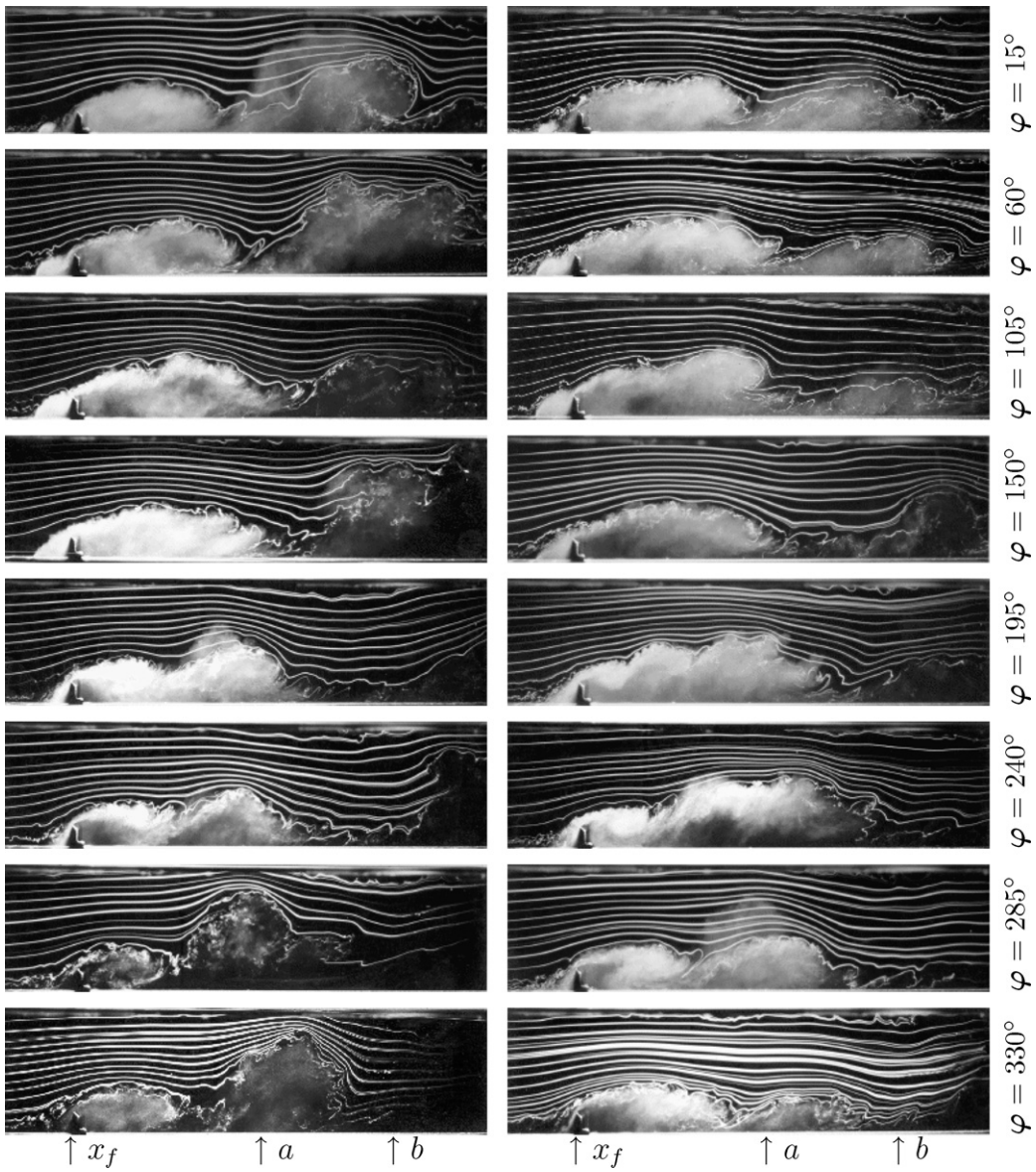

Fig. 9. Phase triggered flow visualisations of the manipulated fence flow, showing two flow states for each phase angle, $15° \leqslant \varphi \leqslant 330°$. Position (a): l_r with, (b): l_r without manipulation.

potential flow above. One finds also that large structures are intermittently being shed from the downstream end of the separation bubble, as can be seen in Fig. 10(b).

The Strouhal number of the shedding type instability (see Eq. (1)) calculated with a shedding frequency of 20 Hz, the free-stream velocity $\overline{u_s}$ at separation and the height of the reverse-flow region, has a value of $St_s \approx 0.08$, which is in accord with Sigurdson [20]. A parameter study with the oscillating jet actuator showed that the forcing frequency associated with the greatest reduction of the reverse-flow region is $f = 21$ Hz.

Fig. 11 shows spectra of the velocity fluctuations calculated from the LDA data for the vertical velocity component for the cases with and without manipulation. The probe was positioned downstream of re-attachment at the outer edge of the shear layer, at

$$x - x_f = 13.5h \quad \text{and} \quad y/h = 4.5.$$

For the flow without manipulation, the shedding of large vortices from the closed reverse-flow region is associated with a broad peak at the shedding frequency of $f \approx 20$ Hz.

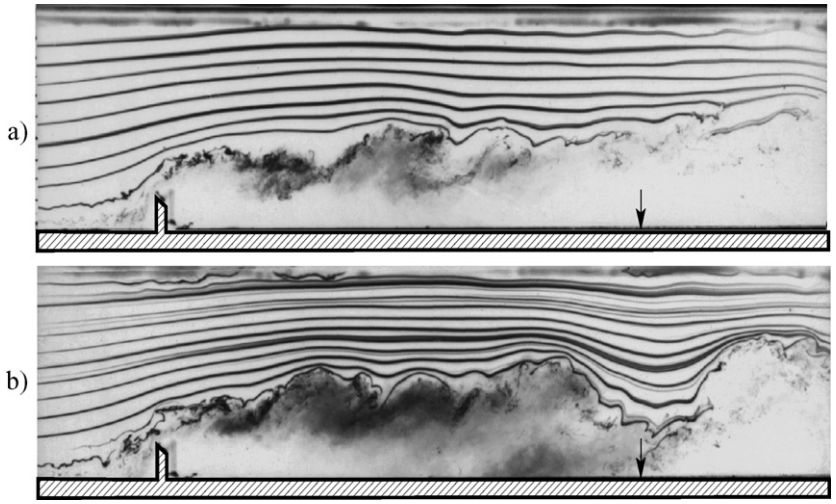

Fig. 10. Smoke-wire flow visualisations of the fence flow without manipulation; the arrows mark the time mean reattachment positions.

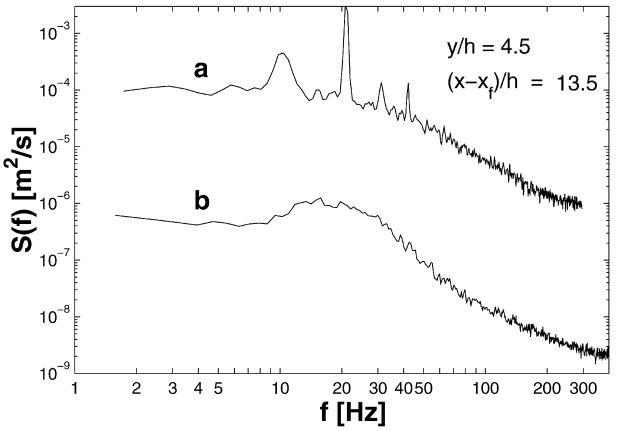

Fig. 11. Frequency spectra of the vertical velocity component at the outer edge of the shear layer for the flow forced with the oscillating jet (a) and for the flow without manipulation (b). The spectra were calculated from the LDA data.

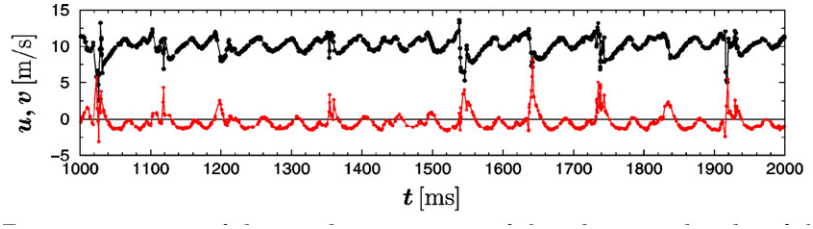

Fig. 12. Time trace of the u and v components of the velocity at the edge of the shear layer measured with the LDA system at $(x - x_f)/h = 6.5$ and $y/h = 3.5$; top: $u(t)$, bottom: $v(t)$.

When the flow is forced at a frequency of $f \approx 21$ Hz, the spectrum shows peaks both at the forcing frequency and its sub-harmonic. Flow visualisations and also time series of the velocity (see Fig. 12) show that this sub-harmonic is the result of a quasi-periodic, intermittent phenomenon.

5. Measurements at the wall

Measurements of the mean and fluctuating pressure and wall-shear stress along the centre line of the test section were compared for the natural flow and the manipulated flow.

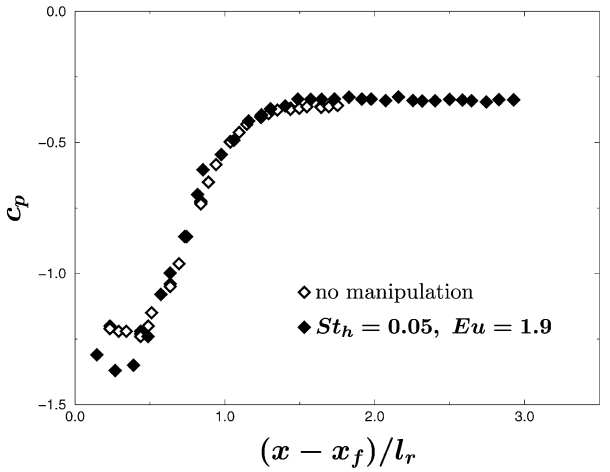

Fig. 13. The pressure distributions downstream of the fence with and without manipulation. The distance from the fence $x - x_f$ is scaled with the length of the reverse-flow region l_r.

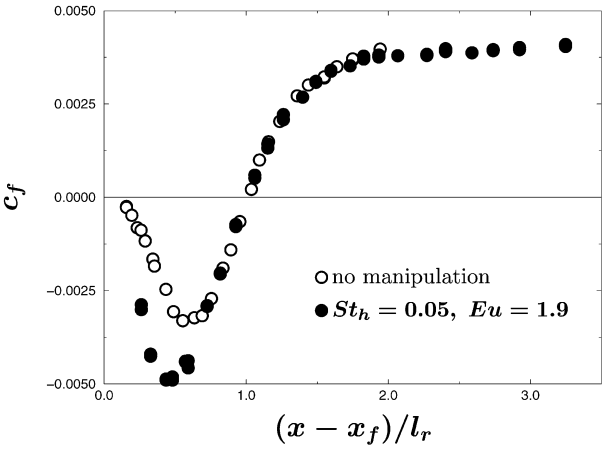

Fig. 14. The wall shear-stress distribution downstream of the fence with and without manipulation. The distance from the fence $x - x_f$ is scaled with the length of the reverse-flow region l_r.

5.1. Mean wall pressure and wall-shear stress

The reduction of the length of the reverse-flow region results in a larger suction peak in the mean wall pressure distribution (Fig. 13) and a lower negative peak in the mean wall shear-stress (Fig. 14). In both figures, the distance from the fence is scaled with the length of the respective reverse-flow region l_r [27]. The pressure and the shear-stress distributions fall on top of each other in this scaling except for the region around and upstream of the suction peak. The suction peak, however, is larger due to the reduced length of the reverse-flow region and the stronger curvature of the streamlines. The free-stream velocity used to normalise c_p and c_f was not affected by the oscillating control flow.

Fig. 15 shows the distribution of the reverse-flow factor χ_w, which was measured by means of a wall pulsed-wire probe. Here, the distance from the fence along the x-axis is scaled with the fence height h, because in this scaling, it is apparent that while for the manipulated flow the length of the reverse-flow region is shorter, the length of the region where reverse-flow events occur is hardly changed.

The re-attachment point is given by $\chi_w = 50\%$ (e.g. Dengel and Fernholz [28]). The reduction of the reverse-flow region is achieved by the strong mixing induced by the large vortices. This is a dynamic phenomenon. The length of the reverse-flow region is only reduced in the time-mean. Instantaneously, the reverse-flow region is broken up into several smaller and weaker regions that travel downstream with the vortices (see the flow visualisations in Fig. 9).

Fig. 16 shows the fluctuating component of the wall shear-stress $c'_f = 2\sqrt{\overline{\tau'^2_w}}/(\rho U_\infty^2)$, which increases from the fence to the time-mean re-attachment position. From there on, c'_f decreases gradually. The maximum values of c'_f in the manipulated case are almost twice as high as in the case without manipulation, while the values far downstream of re-attachment tend towards the undisturbed state of a boundary layer (see Stefes and Fernholz [29]).

The skewness of the wall shear-stress fluctuations $S_w = \overline{\tau'^3}/(\overline{\tau'^2})^{3/2}$ (Fig. 17) has the same sign as τ_w. Therefore, it has negative values inside the reverse-flow region and crosses the zero line at the re-attachment position. For the non-manipulated flow, the skewness has a second zero-crossing that is associated with the secondary separation region immediately downstream of the fence. Also, the negative maximum values indicating strong instantaneous reverse flow events (see Alving and Fernholz [30]) occur in the middle of the reverse-flow region. In the forced case, the values of S_w become positive again closer to the fence.

The slope of the skewness near the time-mean re-attachment line is larger in the case without manipulation than in the manipulated case, where the instantaneous re-attachment position oscillates back and forth over a greater distance. The abscissa of Fig. 17 is scaled with the fence height h to emphasise that downstream of approximately $16h$, S_w is similar for both the manipulated flow and the case without manipulation. This is in line with the behaviour of the reverse-flow factor χ_w and supports the view that the length of the region affected by instantaneous reverse-flow events remains the same. The skewness remains high in the region far downstream of re-attachment for both cases.

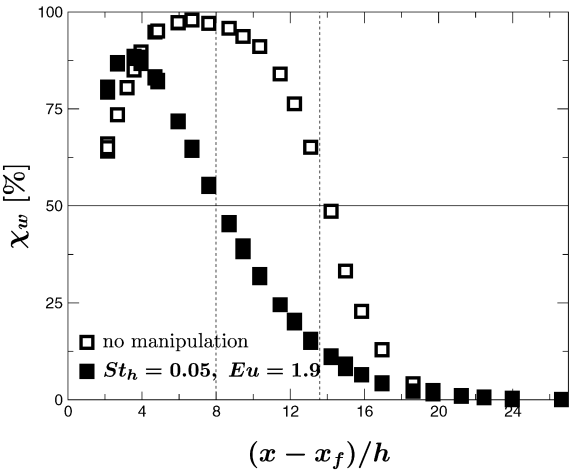

Fig. 15. The distribution of the reverse-flow factor downstream of the fence with and without manipulation. The distance from the fence $x - x_f$ is scaled with the fence height h.

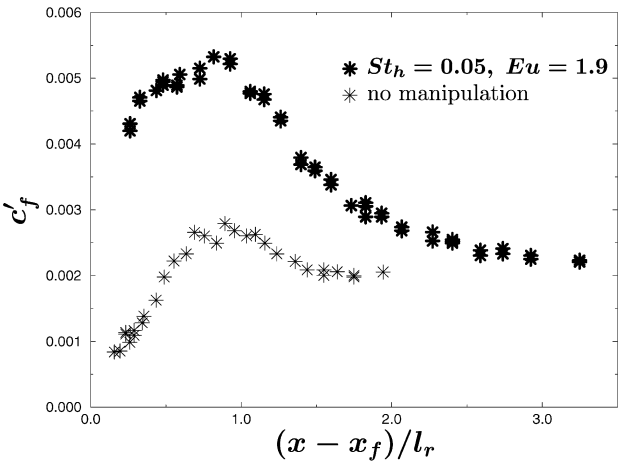

Fig. 16. The fluctuating component of the wall shear-stress downstream of the fence with and without manipulation. The distance from the fence is scaled with the length of the reverse-flow region l_r.

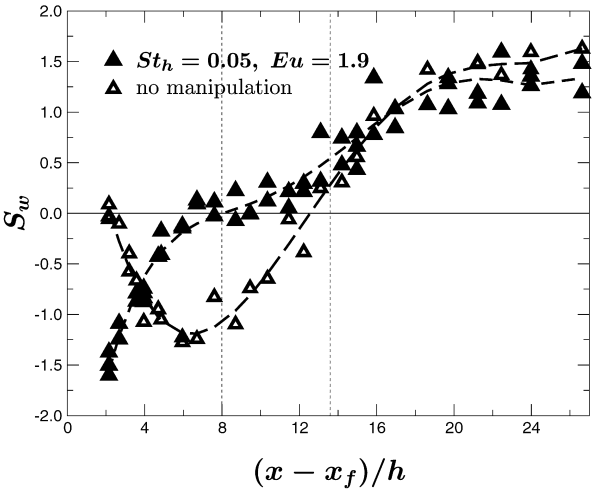

Fig. 17. The skewness S_w of the wall shear-stress fluctuations downstream of the fence with and without manipulation. The distance from the fence is scaled with the fence height h.

These values exceed those of an unperturbed turbulent boundary layer (see Fernholz et al., [31]), because the flow is still highly disturbed.

6. Phase averaged mean velocity and vorticity

Fig. 18 shows the phase averaged velocity field in the region $-2.5h < (x - x_f) < 2.5h$ for four different phase angles φ from 80° to 350° in increments of 90°. Here, the interaction of the oscillating jet emanating from the slot with the separation region upstream of the fence can be studied: during the maximum of the intake movement ($\varphi = 80°$), there is a vortex on the upstream face of the fence with its centre at approximately $x = y = 0.25\ h$. During the maximum outflow phase, a vortex is formed immediately downstream of the slot with almost the height of the fence ($\varphi = 170°$). The flow field upstream of the fence oscillates between these two cases. The periodic growth and decay of a large separated region upstream of the fence displaces the flow over the fence, causing a large starting-type vortex to form (at $\varphi = 170°$) which grows in size as it is convected with the separated shear layer downstream of the fence ($\varphi = 260°$ and 350°).

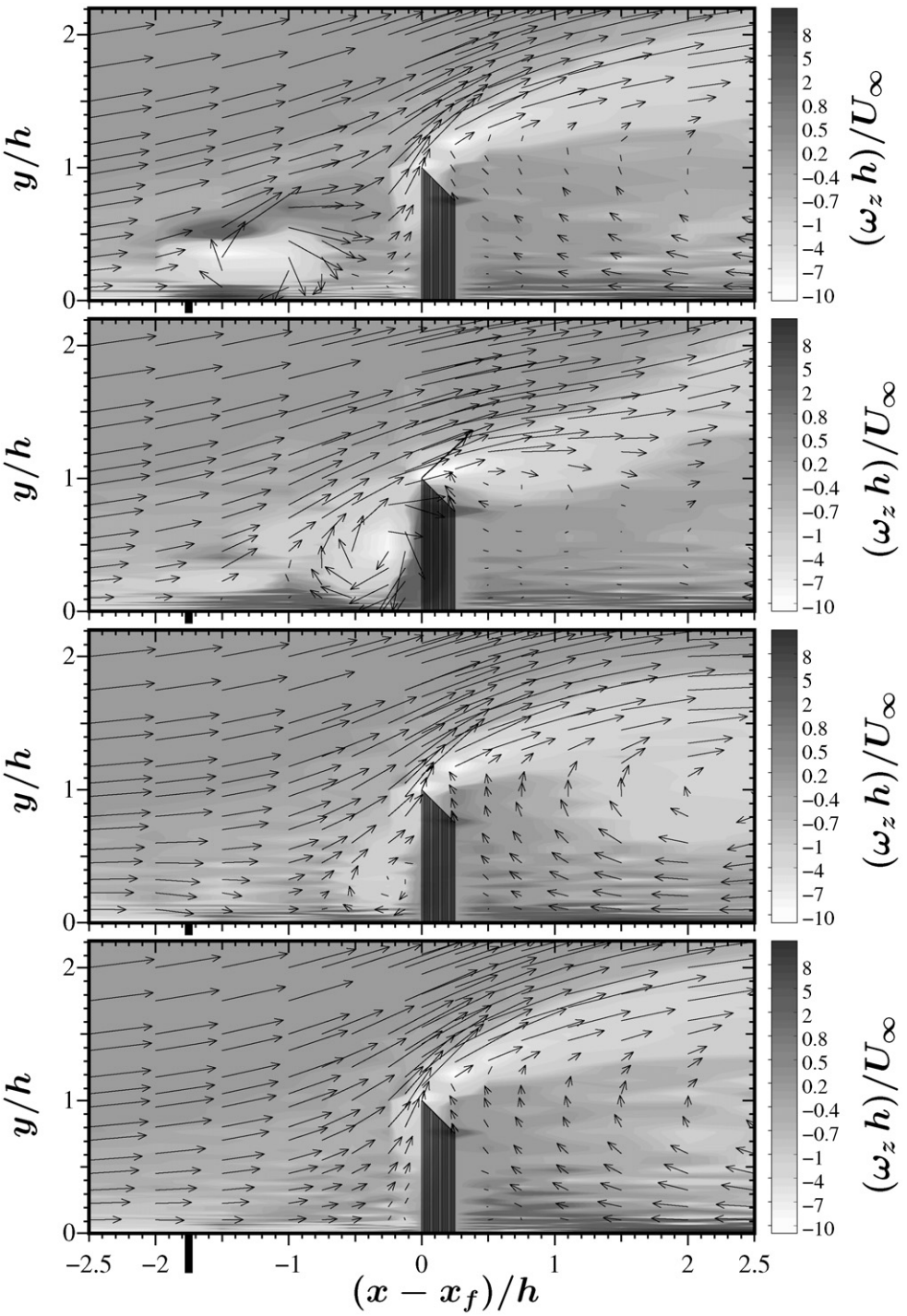

Fig. 18. The phase averaged velocity and vorticity fields up- and downstream of the fence. Phase angles: $\varphi = 80°$, 170°, 260° and 350° from top to bottom, respectively. The actuator slot is located at $(x - x_f)/h = -1.75$.

Fig. 18 is complemented by Fig. 19 that presents the field of streamlines calculated from phase averaged LDA measurements. Both figures show that a continuous train of vortices is convected from the oscillating jet towards the fence and over into the downstream separation region. Upstream of the fence, a vortex forms at the actuator slot at $\varphi = 80°$. It is convected towards the fence and passes over it, cutting the downstream separation region into two at

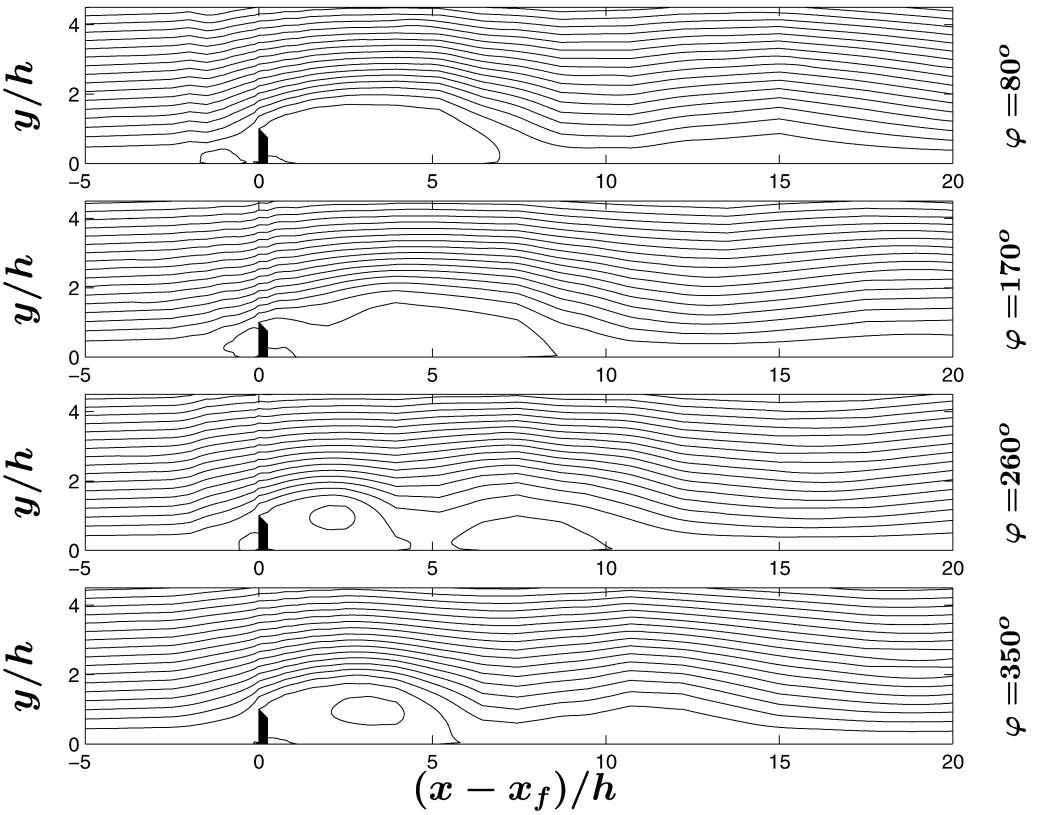

Fig. 19. The phase averaged field of streamlines of the manipulated flow.

$\varphi = 260°$. At the downstream foot of the fence, there exists a secondary separation region that remains in place but oscillates in size. The interaction of the vortices with the fence resembles starting vortices in unsteady flow, e.g. [32]. The instantaneous reattachment line downstream of the fence oscillates up- and downstream so that its time averaged distance from the fence is 40% less than for the non-manipulated flow.

7. Reynolds averaged velocity profiles

Boundary layer profiles in the two flow regimes with the actuator turned on or off were investigated at six different positions $(x - x_f)/l_r = 0.06$, 0.25, 0.48, 0.8, 1.1, and 1.5. The profiles of the streamwise (u) and the vertical (v) velocity components and their fluctuations were measured at different positions along x that are listed in Table 1 together with the values of the streamwise distance from the fence $(x - x_f)$ scaled with the fence height h and the time mean length of the downstream recirculation region when the actuator is on or off ($l_r = 8.0\,h$ for the manipulated flow and $13.6\,h$ for the flow without manipulation). Table 1 also shows the key for Figs. 20 and 21 that present the profiles of the u-component of the velocity, the fluctuations $\overline{u'^2}$, $\overline{u'v'}$, and the turbulence production $\overline{u'v'}\partial u/\partial y$ in dimensionless form.

The profiles of the streamwise velocity component u are shown in Fig. 20. For every profile of the manipulated flow, a corresponding profile measured without manipulation at a position with a similar value of $(x - x_f)/l_r$ is shown (thin solid line). At the first position, closely downstream of the fence where $(x - x_f)/l_r = 0.06$, the profiles are fairly similar for both cases. However, as the flow evolves in the downstream direction, the shear layer becomes thicker and the velocity difference increases for the manipulated flow. The two profiles which are located downstream of the reattachment position ($x = 812$ mm and $x = 882$ mm) are similar again for both cases. Fig. 20 with the turbulent fluctuations $\overline{u'^2}$ and Fig. 21 with $\overline{u'v'}$ show the same trend for the shear layer upstream of reattachment: the shear layer is thicker for the manipulated case and the turbulent fluctuations are stronger and retain higher values downstream of reattachment. The values of $\overline{u'v'}$ relax faster in the downstream direction than those of $\overline{u'^2}$ [4].

Table 1
Key for Figs. 20 and 21; Symbols for the profiles measured at similar values of $(x - x_f)/l_r$ for the flow with and without manipulation

Symbol	Positions where profiles were measured					
	with manipulation			without manipulation		
	x [mm]	$\frac{x-x_f}{h}$	$\frac{x-x_f}{l_r}$	x [mm]	$\frac{x-x_f}{h}$	$\frac{x-x_f}{l_r}$
○	648.0	0.50	0.06	653.0	0.75	0.06
□	678.0	2.00	0.25	702.0	3.20	0.24
◇	717.0	3.95	0.49	767.0	6.45	0.47
△	767.0	6.45	0.81	852.0	10.70	0.79
●	812.0	8.70	1.09	938.0	15.00	1.10
▽	882.0	12.20	1.52	1038.0	20.0	1.47

Profiles of the production of turbulent kinetic energy are presented in Fig. 21. The production occurs mainly within the shear layer. Inside the recirculation region, the production has, however, larger values for the manipulated flow. Downstream of reattachment, the values relax and assume similar values already at the last position, at $(x - x_f)/l_r \approx 1.5$. The values of the production of turbulent kinetic energy integrated in the wall normal direction are shown in Fig. 22. The streamwise coordinate is scaled with the length of the recirculation length. Near the fence, where the profiles of $\bar{u}$ and $\overline{u'v'}$ are fairly similar for the two cases, the integral of the production of turbulent kinetic energy is lower with manipulation, but the values increase rapidly downstream towards a peak of almost twice the height of the case without manipulation. These maximum values occur near $y/h = 0.6$ in the manipulated case and slightly further downstream, near 0.7, for the case without manipulation. Downstream of reattachment, the values of the integral of the production of turbulent kinetic energy for both cases converge until the values are almost equal downstream of $1.5(x - x_f)/l_r$.

The maximum values of the Reynolds stresses continue to grow downstream of the maximum of the production. Fig. 23 presents the maximal values of the Reynolds stresses in the streamwise direction. The values of the Reynolds stresses are scaled according to Brown and Rosko [27] with the local velocity difference in the shear layer Δu. In this scaling, the maximum values occur slightly downstream of reattachment [33] in the centre of the shear layer. The Reynolds stress maxima are much higher when the flow is forced, the maxima of $\overline{u'^2}$ are almost twice as large. The differences between the cases with the actuator on or off grow from the position at the fence to the reattachment position. The differences decrease again in the relaxation region downstream.

Finally, one may note that the turbulence structure is highly anisotropic with $\overline{u'^2}_{\max} > \overline{v'^2}_{\max} > \overline{u'v'}_{\max}$, which has also been reported for similar flow situations, e.g. Ruderich and Fernholz [34] or Hancock and McCluskey [35].

8. Shear-layer thickness

Fig. 24 presents two length-scales for the distance of the shear layer from the floor plate: the half-width $y_{m2} = y(\bar{u} = \bar{u}_{\max}/2)$, i.e. the position where the mean streamwise velocity component has reached half its maximum value, and the height of the shear layer $y_{\Delta\bar{u}/2} = y(\bar{u} = \Delta\bar{u}/2)$, where the mean streamwise velocity component has reached a value of half the velocity difference across the shear layer $\Delta\bar{u} = \bar{u}_{\max} - \bar{u}_{\min}$. When the flow is manipulated, the shear layer is closer to the wall because entrainment is increased by the higher vorticity.

Other length-scales which characterise free shear layers are the displacement thickness δ^* and the momentum thickness θ (see Fig. 25). For a shear layer, the displacement thickness is defined as (Batchelor [36], e.g.)

$$\delta^* = \int_{-\infty}^{\infty} \left(1 - \frac{\bar{u} - \bar{u}_{\min}}{\bar{u}_{\max} - \bar{u}_{\min}}\right) \mathrm{d}y, \tag{2}$$

and the momentum thickness of a shear layer as

$$\theta = \int_{-\infty}^{\infty} \left(\frac{\bar{u} - \bar{u}_{\min}}{\bar{u}_{\max} - \bar{u}_{\min}} \left[1 - \frac{\bar{u} - \bar{u}_{\min}}{\bar{u}_{\max} - \bar{u}_{\min}}\right]\right) \mathrm{d}y \tag{3}$$

(e.g. Gaster et al. [37]). The velocity profiles are integrated from $y(\bar{u}_{\min})$ to $y(\bar{u}_{\max})$.

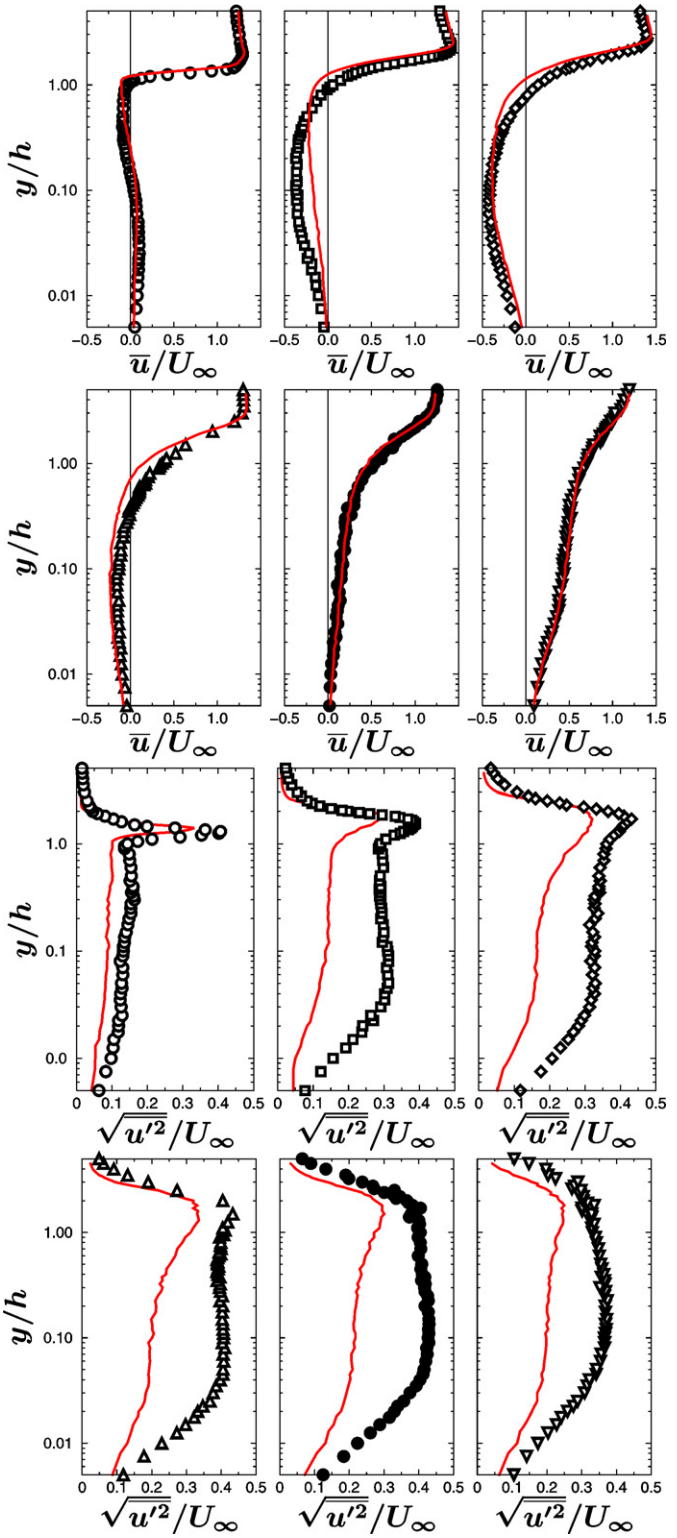

Fig. 20. Profiles of $\bar{u}/U_\infty$ and $\sqrt{\overline{u'^2}}/U_\infty$ at six x-positions measured along the centre-line of the test section downstream of the fence. Symbols see Table 1; solid line: flow without manipulation.

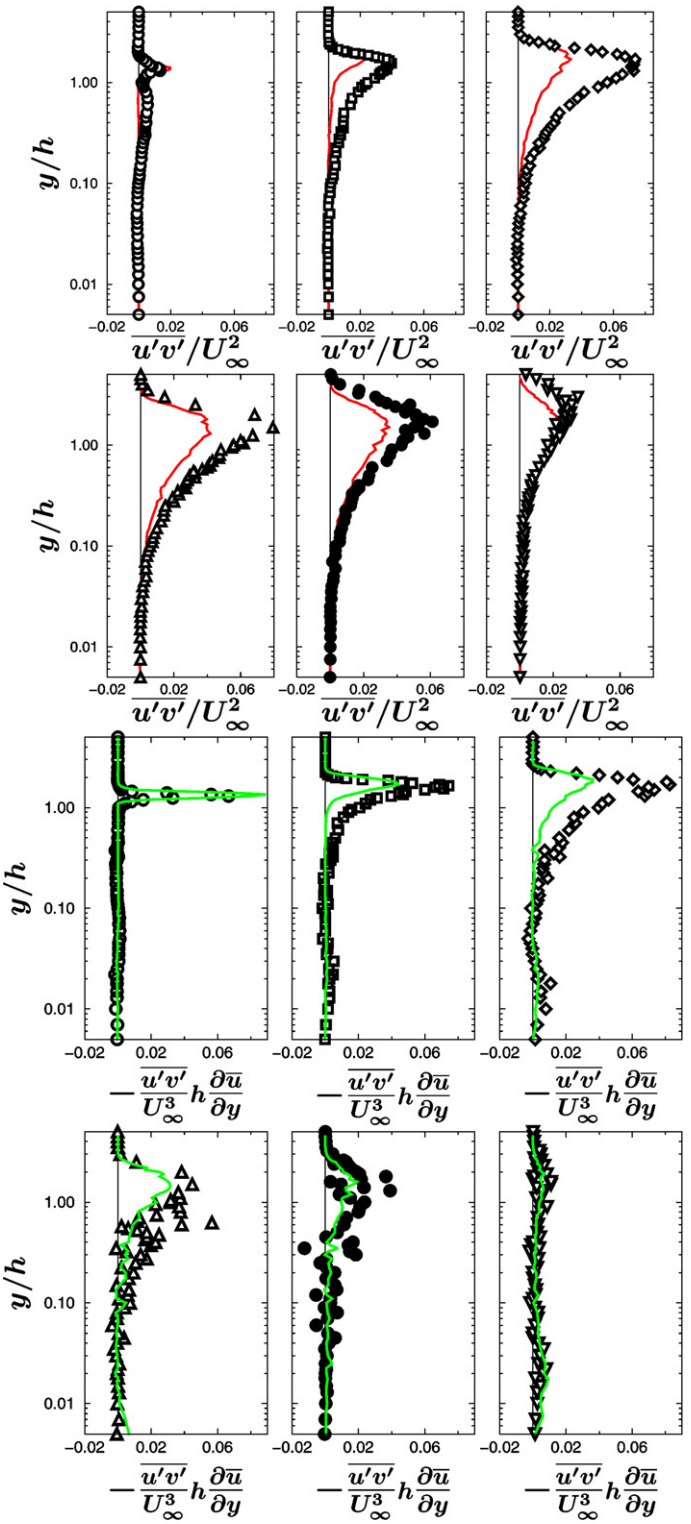

Fig. 21. Profiles of $\overline{u'v'}/U_\infty^2$ and the production of turbulent kinetic energy at six positions along the centre-line of the test section. Symbols see Table 1; solid line: flow without manipulation.

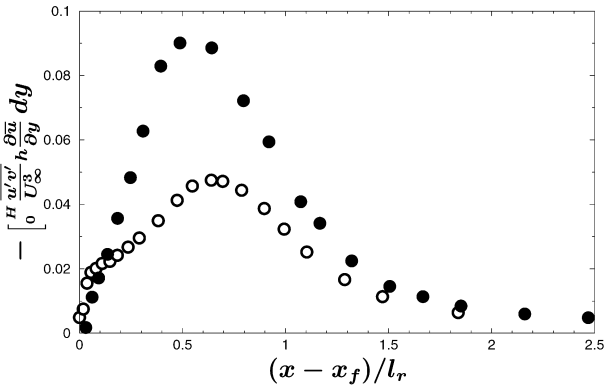

Fig. 22. Development of the integral of the production of turbulent kinetic energy; solid symbols with and open symbols without manipulation.

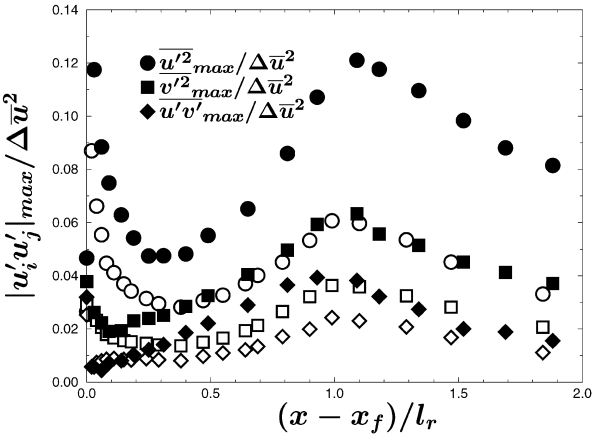

Fig. 23. Development of the maxima of the specific Reynolds stresses scaled with the velocity difference across the shear layer $\Delta\bar{u}$; solid symbols: with manipulation, open symbols: without manipulation.

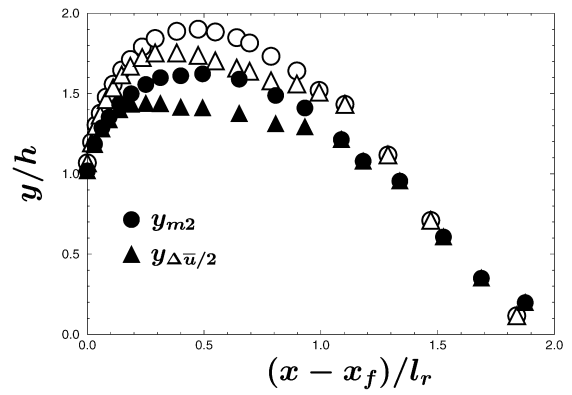

Fig. 24. Development of the half-width y_{m2} and the shear layer height $y_{\Delta\bar{u}/2}$; solid symbols: with manipulation, open symbols: without manipulation.

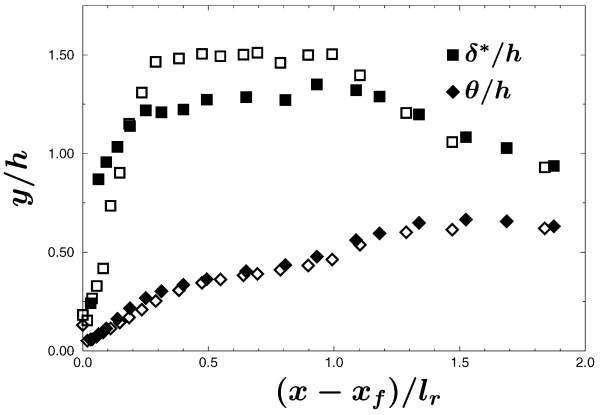

Fig. 25. Development of the displacement thickness δ^* and the momentum thickness θ of the shear-layer downstream of the fence; solid symbols: with manipulation, open symbols: without manipulation.

Downstream of the fence, δ^* grows faster for both cases than θ because it reacts stronger to changes in the boundary conditions [28]. When the shear layer has reached its highest point above the floor plate, the displacement thickness reaches a plateau. The values of the displacement thickness δ^* are higher in the manipulated case, because the increased entrainment brings the shear layer closer to the floor plate. Downstream of the reattachment line, the values of δ^* decrease and those of θ increase and then remain approximately constant.

The vorticity thickness defined by Brown and Roshko [27] is

$$\delta_\omega = \frac{\bar{u}_{\max} - \bar{u}_{\min}}{(\partial\bar{u}/\partial y)_{\max}}.$$

The vorticity thickness grows more rapidly and assumes larger values in the manipulated case than in the case without manipulation (see Fig. 26). δ_ω grows rapidly from the fence tip on downstream and its growth rate $\mathrm{d}\delta_\omega/\mathrm{d}x$ is 0.44 for the case with manipulation and 0.27 for the case without manipulation. Downstream of $(x - x_f)/l_r \approx 0.6$, the growth rate for the manipulated flow is reduced to 0.18, a value found in the plane mixing layer (e.g. Eaton and Johnston [38] or Ruderich and Fernholz [34]). In the centre of the reverse flow region, between $0.2 < (x - x_f)/l_r < 0.7$, the shear layer in the flow without manipulation has a slightly lower growth rate of 0.17 in agreement with values for plane mixing layers (see [39] and [40]).

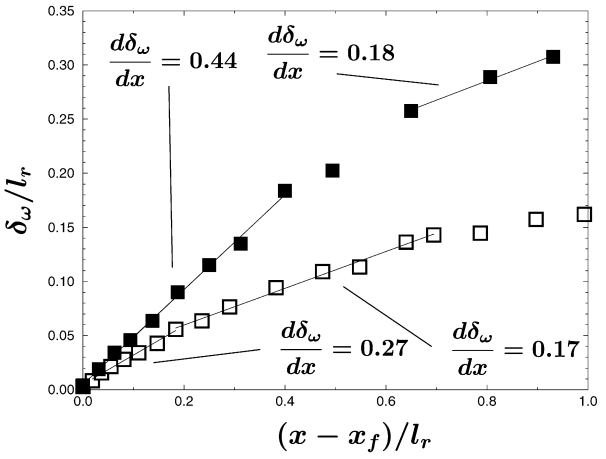

Fig. 26. Development of the vorticity thickness δ_ω along the centre-line; solid symbols: with manipulation, open symbols: without manipulation.

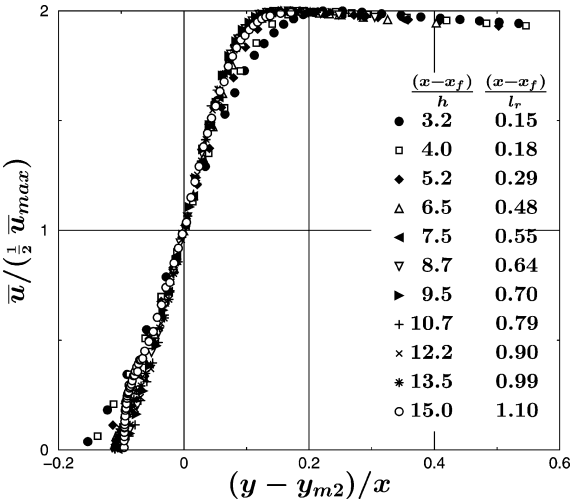

Fig. 27. Mean velocity profiles of the shear layer scaled with $0.5\bar{u}_{\max}$ and the half-width y_{m2} (no manipulation).

9. Velocity profiles in shear-layer scaling

Fig. 27 presents mean velocity profiles for the flow without manipulation in shear-layer scaling with $\bar{u}_{\max}/2$ as reference velocity and $(y - y_{m2})/x$ as non-dimensional length scale. In this scaling, as proposed by Wygnanski and Fiedler [41], the mean velocity profiles in the shear layer show a self-similar region in the core area of the shear layer, where $0.5 \leqslant 2\bar{u}/\bar{u}_{\max} \leqslant 1.5$.

The profiles measured with manipulation, shown in Fig. 28, do not show such a self-similar region, but collapse onto each other apart from the near-wall region.

9.1. The boundary layer downstream of re-attachment

Downstream of reattachment, the boundary layer recovers from the severe disturbance. Figs. 29 (for the case without manipulation) and 30 (with manipulation) show this recovery of the mean velocity profiles towards a turbulent zero-pressure gradient boundary layer in inner layer scaling. A comparison of the values of u^+ at different positions of $(x - x_f)/l_r$ for constant values of u^+ shows that the recovery towards the logarithmic law is faster in the manipulated case. According to Alving and Fernholz [30], the minimum length necessary until the canonical profile (e.g. Fernholz and Finley [42]) is reached is $6l_r$.

The inner layer of the mean velocity profiles presented in Figs. 29 and 30 is heavily distorted, but the mean velocity profiles approach the logarithmic law of the wall in downstream direction. At the position furthest downstream where a boundary layer profile could be measured, at $(x - x_f) = 25\,h$, the profile with manipulation coincides almost with the logarithmic law, whereas the profile without manipulation still deviates from it.

Profiles of $\sqrt{\overline{u'^2}}/u_\tau$ are shown in Figs. 31 (without manipulation) and 32 (with manipulation). The reference profile, shown as a dotted line in Figs. 31 and 32, was measured on the flat plate at the fence position with the fence removed. The levels of $\sqrt{\overline{u'^2}}/u_\tau$ decrease in the streamwise direction, but the maximum values of $\sqrt{\overline{u'^2}}/u_\tau$ are still at the outer edge of the wall bounded shear flow. The recovery of the turbulence structure to that of a canonical boundary layer is still far away, since the large structures shed from the reverse flow region and the upstream shear layer dominate the flow [30].

10. Conclusions

The reverse-flow region upstream and downstream of a fence on a flat plate was investigated with and without manipulation by an oscillating spoiler and a zero mass-flux actuator. The Reynolds number based on the free-stream velocity and fence height was $Re_h = 10\,500$, blockage of the test section by the fence was $H/h = 6.75$.

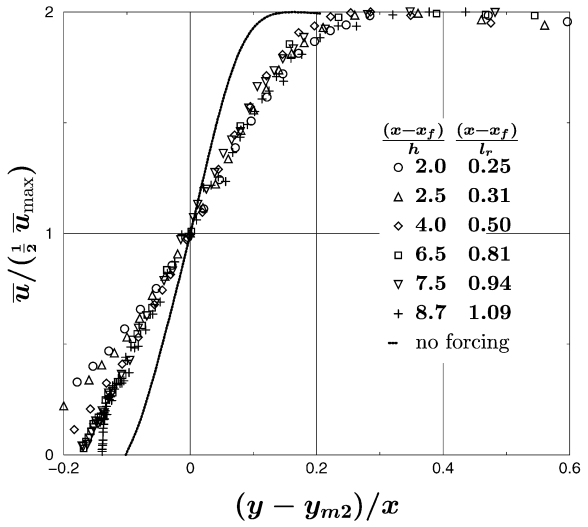

Fig. 28. Mean velocity profiles of the manipulated flow in shear-layer scaling. The solid line represents the mean velocity profile for the case without manipulation.

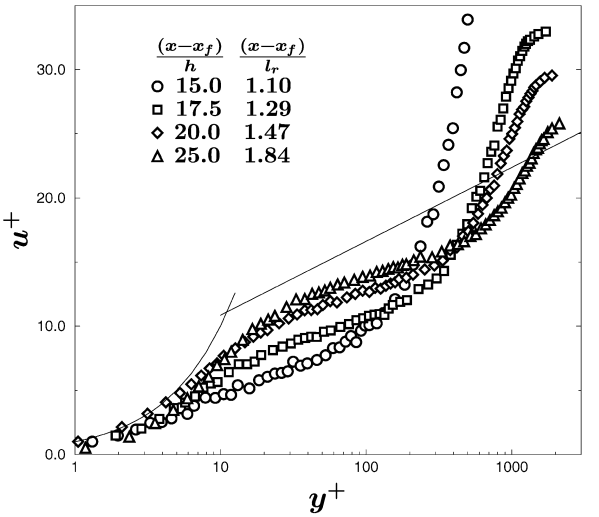

Fig. 29. Mean velocity profiles in wall coordinates downstream of re-attachment (no manipulation).

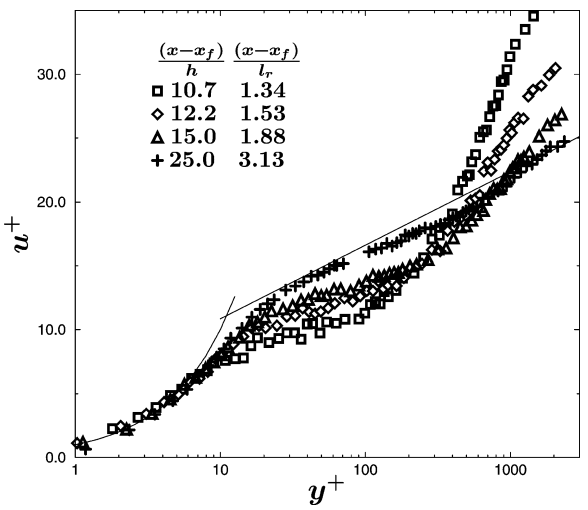

Fig. 30. Mean velocity profiles in wall coordinates downstream of re-attachment (with manipulation).

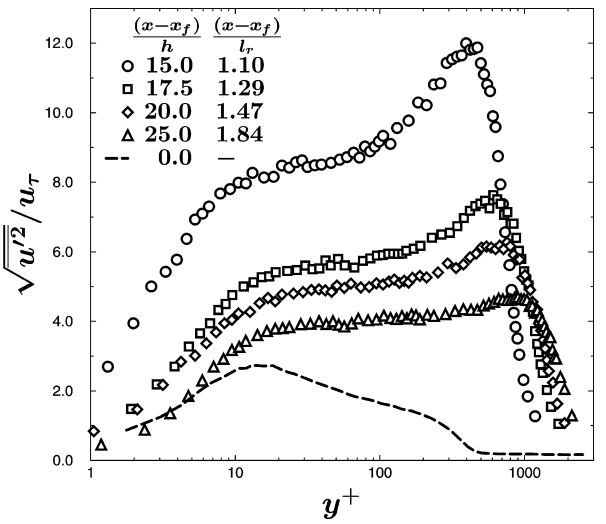

Fig. 31. Profiles of $\sqrt{\overline{u'^2}}/u_\tau$ downstream of reattachment (no manipulation); - - - reference profile measured at the fence position with the fence removed.

The time mean length of the recirculation region downstream of the fence can be reduced when a periodical disturbance is introduced upstream of the recirculation zone that is situated upstream of the fence. Two different types of actuators, a mechanical oscillating spoiler and a zero net mass-flux actuator, were used. Both actuators had the same effect, but the latter was easier to control and to handle. Therefore, detailed flow measurements were performed only for the zero net mass-flux actuator, while the flow with the oscillating spoiler was only analysed using flow visualisation.

The parameters of the actuator, its position upstream of the fence, frequency and amplitude, were optimised. The optimal position is just upstream of the separation point in front of the fence, the optimal frequency is the natural shedding frequency of the downstream separation region. The amplitude of the actuator was limited and a saturated state where a further increase of the amplitude would have made the recirculation increase again could not be reached.

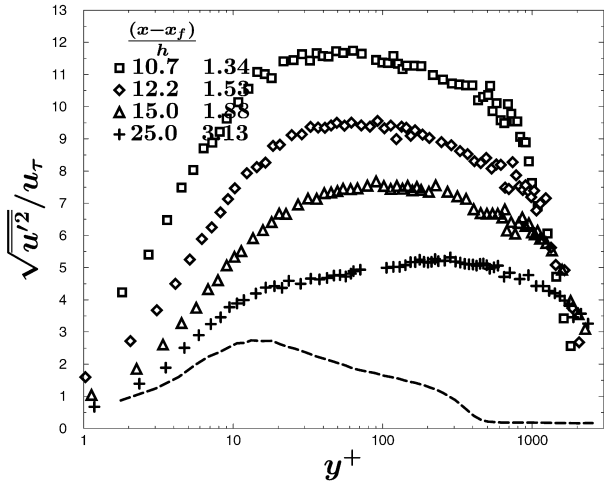

Fig. 32. Profiles of $\sqrt{\overline{u'^2}}/u_\tau$ downstream of re-attachment (with manipulation); - - - reference profile measured at the fence position with the fence removed and without manipulation.

With the optimised manipulation conditions, the time mean length of the separation region downstream of the fence is reduced from $13.6h$ to $l_r = 8.0h$.

For the case with the zero net mass-flux actuator, measurements were performed of the profiles of the streamwise and vertical velocity components, measured with an LDA system, of the wall shear-stress and the reverse-flow parameter, measured with a wall pulsed-wire probe, and of the wall pressure.

Visualisations of the flow show large vortical structures in the shear layer downstream of the fence. Spectra of the velocity measured at the edge of the shear layer near reattachment show a broad peak between 10 and 30 Hz. The growth rate of the mixing layer is initially larger than a plane mixing layer but it approaches its development further downstream. The shear layer is curved, rising upward until the middle of the recirculation region and than curving back towards the floor plate.

When the actuator is off, the wall shear-stress measurements show that the recirculation region downstream of the fence is a strong recirculation region [7]: the reverse flow factor $\chi_w > 90\%$, the distributions of the (negative) time mean wall shear stress and the mean wall pressure have large gradients, and the fluctuating components of wall shear-stress are large. The wall shear stress fluctuations and the Reynolds stresses reach maximum values just upstream of reattachment.

The optimal forcing frequency coincides with the shedding frequency of the reverse-flow region for the case where the actuator is off. The optimal Strouhal number (see Eq. (1)), calculated with the free-stream velocity at separation, i.e. at the fence, and the maximum time mean height of the separation region, $St_s = 0.08$ has the numerical value of a shedding type instability described by Sigurdson [20].

While the time mean length of the reverse-flow region is reduced by the manipulation, the length of the region where reverse-flow events occur remains unchanged (see Figs. 15 and 17).

Downstream of the time mean reattachment position, a new boundary layer develops. The mean velocity profiles relax towards the logarithmic velocity law, while the profiles of the turbulent fluctuations still remain far from the values in a canonical turbulent boundary layer.

References

[1] H. Siller, H. Fernholz, Separation behaviour in front of a two-dimensional fence, Eur. J. Mech. B Fluids 20 (2001) 727–740.
[2] H. Siller, Reduction of the Recirculation Length Downstream of a Fence by an Oscillating Cross-Flow, Mensch und Buch Verlag, Berlin, 1999. Dissertation, TU-Berlin (D83), ISBN 3-89820-038-8.
[3] H.A. Siller, H.-H. Fernholz, Control of separated flow downstream of a two-dimensional fence by low-frequency forcing, Appl. Scientific Res. 57 (1997) 309–318.
[4] A. Huppertz, H. Fernholz, Active control of the turbulent flow over a swept fence, Eur. J. Mech. B Fluids 21 (2002) 425–446.
[5] Simpson, R. L., Two-dimensional turbulent separated flow, AGARDograph 287, AGARD, 1985.

[6] P.E. Hancock, Measurements of mean and fluctuating wall shear stress beneath spanwise-invariant separation bubbles, Exp. Fluids 27 (1) (1999) 53–59.
[7] H.H. Fernholz, Near-wall phenomena in turbulent separated flows, Acta Mech. 4 (1994) 57–67.
[8] M.C. Good, P.N. Joubert, The form drag of two-dimensional bluff-plates immersed in turbulent boundary layers, J. Fluid Mech. 31 (3) (1968) 547–582.
[9] K. Ranga Raju, J. Loeser, E.J. Plate, Velocity profiles and fence drag for a turbulent boundary layer along smooth and rough flat plates, J. Fluid Mech. 76 (2) (1976) 383–399.
[10] I.P. Castro, J.E. Fackrell, A note on two-dimensional fence flows, with emphasis on wall constraints, J. Industrial Aerodynamics 3 (1978) 1–20.
[11] F. Durst, A.K. Rastogi, Turbulent flow over two-dimensional fences, in: L.J.S. Bradbury, F. Durst, B.E. Launder, F.W. Schmidt, J.H. Whitelaw (Eds.), in: Turbulent Shear Flows, vol. II, Springer, 1980, pp. 218–232.
[12] A. Žukauskas, A. Pedišius, Free-stream turbulence effects on the heat transfer through the turbulent boundary layer behind a fence, Int. Comm. Heat Mass Transfer 10 (1983) 277–286.
[13] P.M. Wagner, Kohärente Strukturen der Turbulenz im wandnahen Bereich von Ablösegebieten. Ph.D. thesis, Technische Universität Berlin, 1994.
[14] J.J. Schmidt, Experimental and numerical investigation of separated flows. Ph.D. thesis, Danmarks Tekniske Universitet, 1997.
[15] U. Ullum, J.J. Schmidt, P.S. Larsen, D.R. McCluskey, Temporal evolution of the perturbed and unperturbed flow field behind a fence: PIV analysis and comparison with LDA data, in: 7th International Conference on Laser Amemometry Advances and Applications. Karlsruhe, Germany, 8–12 September 1997.
[16] H.A. Siller, H.-H. Fernholz, Turbulent separation regions in front and downstream of a fence, in: S. Gavrilakis, L. Machiels, P.A. Monkewitz (Eds.), Advances in Turbulence, vol. VI, Kluwer Academic Press, 1996, pp. 487–490.
[17] A. Orellano, Grobstruktursimulation der Umströmung eines Zaunes in einer turbulenten Grenzschicht. Arbeitsbericht zum Forschungsvorhaben WE 705/4-2 98/2, Institut für Strömungsmechanik und Aerodynamik, Universität der Bundeswehr München, 1998.
[18] M. Gad-el Hak, D.M. Bushnell, Separation control: review, J. Fluids Engrg. 113 (1991) 5–30.
[19] A. Orellano, H. Wengle, Numerical simulation (dns and les) of manipulated turbulent boundary layer flow over a surface-mounted fence, Eur. J. Mech. B Fluids 19 (2000) 765–788.
[20] L.W. Sigurdson, The structure and control of a turbulent reattaching flow, J. Fluid Mech. 298 (1995) 139–165.
[21] J.J. Miau, J.H. Chou, Frequency effect of an oscillating plate immersed in a turbulent boundary layer, AIAA J. 29 (7) (1991) 1068–1074.
[22] J.J. Miau, C.R. Chen, J.H. Chou, A vertically oscillating plate disturbing the development of a boundary layer, J. Fluid Mech. 298 (1995) 1–22.
[23] K.B. Chun, H.J. Sung, Control of turbulent separated flow over a backward-facing step by local forcing, Exp. Fluids 21 (1996) 417–426.
[24] L.J.S. Bradbury, I.P. Castro, A pulsed-wire technique for velocity measurements in highly turbulent flow, J. Fluid Mech. 22 (1971) 679–687.
[25] I.P. Castro, Pulsed-wire anemometry, Exp. Therm. Fluid Sci. 5 (1992) 770–780.
[26] V.C. Patel, Calibration of the Preston tube and limitations on its use in pressure gradients, J. Fluid Mech. 23 (1965) 185–208.
[27] G.L. Brown, A. Roshko, On density effects and large structure in turbulent mixing layers, J. Fluid Mech. 64 (1974) 775–886.
[28] P. Dengel, H.-H. Fernholz, An experimental investigation of an incompressible turbulent boundary layer in the vicinity of separation, J. Fluid Mech. 212 (1990) 615–636.
[29] B. Stefes, H.-H. Fernholz, Skin friction and turbulence measurements in a boundary layer with zero-pressure-gradient under the influence of high intensity free-stream turbulence, Eur. J. Mech. B Fluids 23 (2) (2004) 303–318.
[30] A.E. Alving, H.H. Fernholz, Turbulence measurements around a mild separation bubble and downstream of reattachment, J. Fluid Mech. 322 (1996) 297–328.
[31] H.-H. Fernholz, G. Janke, M. Schober, P.M. Wagner, D. Warnack, New developments and applications of skin-friction measuring techniques, Meas. Sci. Technol. 7 (1996) 1396–1409.
[32] F. Finaish, P. Freymuth, W. Bank, Starting flow over spoilers, double steps and cavities, J. Fluid Mech. 168 (1986) 383–392.
[33] M. Kiya, K. Sasaki, Structure of a turbulent separation bubble, J. Fluid Mech. 137 (1983) 83–113.
[34] R. Ruderich, H.H. Fernholz, An experimental investigation of the structure of a turbulent shear flow with separation, reverse flow, and reattachment, J. Fluid Mech. 163 (1986) 283–322.
[35] P.E. Hancock, F.M. McCluskey, Spanwise-invariant three-dimensional separated flow, Experimental Thermal and Fluids Science 14 (1997) 25–43.
[36] G.K. Batchelor, An Introduction to Fluid Dynamics, Cambridge University Press, 1967.
[37] M. Gaster, E. Kit, I. Wygnanski, Large-scale structures in a forced turbulent mixing layer, J. Fluid Mech. 150 (1995) 23–39.
[38] J.K. Eaton, J.P. Johnston, Turbulent flow reattachment: An experimental study of the flow and structure behind a backward-facing step. Tech. Rep. MD-39, Stanford University, 1980.
[39] T.R. Troutt, B. Scheelke, T.R. Norman, Organized structures in a reattaching separated flow field, J. Fluid Mech. 143 (1984) 413–427.
[40] G. Dimaczek, R. Kessler, R. Martinuzzi, C. Tropea, The flow over two-dimensional, surface mounted obstacles at high Reynolds numbers, in: Proc. 7 th Symposium on Turbulent Shear Flows, Stanford, CA, 1989, pp. 10.1.1–10.1.6.
[41] I. Wygnanski, H.E. Fiedler, The two-dimensional mixing region, J. Fluid Mech. 41 (1970) 327–361.
[42] H.H. Fernholz, P.J. Finley, The incompressible zero-pressure-gradient turbulent boundary layer: An assessment of the data, Prog. Aerospace Sci. 32 (1996) 245–311.